INTERNATIONAL JOURNAL OF
ENERGY AND ENVIRONMENT

Volume 3, Issue 3, 2012 pp.359-382

Journal homepage: www.IJEE.IEEFoundation.org

Hamilton–Jacobi–Bellman equations and dynamic programming for power-optimization of radiative law multistage heat engine system

Shaojun Xia, Lingen Chen, Fengrui Sun

College of Naval Architecture and Power, Naval University of Engineering, Wuhan 430033, P. R. China.

Abstract

A multistage endoreversible Carnot heat engine system operating with a finite thermal capacity high-temperature black photon fluid reservoir and the heat transfer law [$q \propto \alpha(T^{4-n})(\Delta(T^n))$] is investigated in this paper. Optimal control theory is applied to derive the continuous Hamilton-Jacobi-Bellman (HJB) equations, which determine the optimal fluid temperature configurations for maximum power output under the conditions of fixed initial time and fixed initial temperature of the driving fluid. Based on the general optimization results, the analytical solution for the case with pseudo-Newtonian heat transfer law [$q \propto \alpha(T^3)(\Delta T)$] is further obtained. Since there are no analytical solutions for the radiative heat transfer law [$q \propto \Delta(T^4)$], the continuous HJB equations are discretized and the dynamic programming (DP) algorithm is adopted to obtain the complete numerical solutions, and the relationships among the maximum power output of the system, the process period and the fluid temperatures are discussed in detail. The optimization results obtained for the radiative heat transfer law are also compared with those obtained for pseudo-Newtonian heat transfer law and stage-by-stage optimization strategy. The obtained results can provide some theoretical guidelines for the optimal designs and operations of solar energy conversion and transfer systems.

Keywords: Radiative heat transfer law; Multistage heat engine system; Maximum power; Optimal control; Finite time thermodynamics.

1. Introduction

There are two standard problems in finite time thermodynamics [1-12]: one is to determine the objective function limits and the relations between objective functions for the given thermodynamic system, and another is to determine the optimal thermodynamic process for the given optimization objectives. The former case belongs to a class of static optimization problems, which could be solved by the simple function derivation methods, while the latter case belongs to a class of dynamic optimization problems, which should be solved by applying optimal control theory. Sieniutycz [5, 7, 11, 13-16], Sieniutycz and von Spakovsky [17], Szwast and Sieniutycz [18] first investigated the maximum power output of multistage continuous endoreversible Carnot heat engine system operating between a finite thermal capacity high-temperature fluid reservoir and an infinite thermal capacity low-temperature environment with Newtonian heat transfer law [5, 7, 11, 13-15, 17]. The results were extended to the multistage discrete endoreversible Carnot heat engine system [5, 7, 11, 16, 18]. Sieniutycz and Szwast [19],

Sieniutycz [20] further investigated effects of internal irreversibility on the maximum power output of multistage Carnot heat engine system and the corresponding optimal fluid reservoir temperature configuration. Li *et al* [21, 22] further considered that both the high- and low-temperature sides are finite thermal capacity fluid reservoirs, and investigated the problems of maximizing the power output of multistage continuous endoreversible [21] and irreversible [22] Carnot heat engine systems with Newtonian heat transfer law. In general, heat transfer is not necessarily Newtonian heat transfer law and also obeys other laws. Heat transfer laws not only have significant influences on the performance of the given thermodynamic process [23-27], but also have influences on the optimal configurations of thermodynamic process for the given optimization objectives [28-33]. Sieniutycz and Kuran [34, 35], Kuran [36] and Sieniutycz [11, 37-40] investigated the maximum power output of the finite high-temperature fluid reservoir multistage continuous irreversible Carnot heat engine system with the radiative heat transfer law and the corresponding optimal fluid reservoir temperature configuration. Because there are no analytical solutions for the case with the pure radiative heat transfer law, Refs. [11, 35-40] obtained the analytical solutions of the optimization problems by replacing the radiative heat transfer law by the so called pseudo-Newtonian heat transfer law [$q \propto \alpha(T^3)(\Delta T)$] approximately, which is Newtonian heat transfer law with a heat transfer coefficient $\alpha(T^3)$ as a function of the cube of the fluid reservoir temperature. Sieniutycz [41] further investigated the maximum power output of multistage continuous irreversible Carnot heat engine system with the non-linear heat transfer law [$q \propto \alpha(T^n)(\Delta T)$], i.e. Newtonian heat transfer law with a heat transfer coefficient $\alpha(T^n)$ as a function of the *n*-times of the fluid reservoir temperature. Li *et al.* [42] further investigated the problems of maximizing the power output of multistage continuous endoreversible Carnot heat engine system with two finite thermal capacity heat reservoirs and the pseudo-Newtonian heat transfer law. Xia *et al.* [43, 44] investigated the maximum power output of the multistage continuous endoreversible [43] and irreversible [44] Carnot heat engine system with the generalized convective heat transfer law [$q \propto (\Delta T)^m$], and obtained different results from those obtained in Refs. [5, 7, 11, 13-22, 34-42]. On the basis of Refs. [5, 7, 11, 13-22, 34-44], this paper will further investigate the maximum power output of multistage endoreversible Carnot heat engine system, in which the heat transfer between the reservoir and the working fluid obeys the heat transfer law [$q \propto \alpha(T^{4-n})(\Delta(T^n))$]. Based on the general optimization results, the analytical solution for the case with pseudo-Newtonian heat transfer law ($\mathrm{n}=1$) will be further obtained. While for the case with the radiative heat transfer law ($\mathrm{n}=4$), the continuous HJB equations will be discretized and the dynamic programming (DP) method will be performed to obtain the complete numerical solutions of the optimization problem.

2. System modeling and characteristic description

2.1 Fundamental characteristic of a single-stage stationary endoreversible Carnot heat engine

Each infinitesimal endoreversible Carnot heat engine as shown in Figure 1 is assumed to be a single stage endoreversible Carnot heat engine with stationary heat reservoirs. Let the heat flux rates absorbed and released by the working fluid in the heat engine be q_1 and q_2, respectively. T_1 and T_2 are the reservoir temperatures corresponding to the high- and low-temperature sides, respectively. $T_{1'}$ and $T_{2'}$ are the temperatures of the working fluid corresponding to the high- and low-temperature sides, respectively. Considering that the heat transfer between the reservoir and the working fluid obeys the radiative heat transfer law, then

$$q_1 = k_1(T_1^4 - T_{1'}^4), \quad q_2 = k_2(T_{2'}^4 - T_2^4) \tag{1}$$

where k_1 and k_2 are the heat conductances of heat transfer process corresponding to high- and low-temperature sides, which is related to Stefan-Boltzmann constant and heat transfer surface area. If the differences between T_1 and $T_{1'}$ as well as $T_{2'}$ and T_2 are small, Eq. (1) can be further expressed as [45]

$$q_1 = 4k_1T_1^3(T_1 - T_{1'}), \quad q_2 = 4k_2T_2^3(T_{2'} - T_2) \tag{2}$$

Eq. (2) can be regarded as Newtonian heat transfer law with a conductance as a function of T^3, which is called pseudo-Newtonian heat transfer law in Refs. [5, 31-36]. In order to compare optimization results for these two different heat transfer laws, Eqs. (1) and (2) can be expressed as

$$q_1 = (5-n)k_1 T_1^{4-n}(T_1^n - T_{1'}^n), \quad q_2 = (5-n)k_2 T_2^{4-n}(T_{2'}^n - T_2^n) \tag{3}$$

From Eqs. (1)-(3), one can see that when $n=1$ Eq. (3) turns to be pseudo-Newtonian heat transfer law of Eq. (2); when $n=4$, Eq. (3) turns to be Stefan-Boltzmann radiative heat transfer law of Eq. (1). Since the heat engine is an end reversible one, one further obtains entropy balance equation from the second law of thermodynamics as follows

$$k_1 T_1^{4-n}(T_1^n - T_{1'}^n)/T_{1'} = k_2 T_2^{4-n}(T_{2'}^n - T_2^n)/T_{2'} \tag{4}$$

From Eqs. (3) and (4), the power output P and the efficiency η of the heat engine are given by

$$P = q_1 - q_2 = q_1\eta \tag{5}$$

$$\eta = P/q_1 = 1 - q_2/q_1 = 1 - T_{2'}/T_{1'} \tag{6}$$

The main irreversibility of the endoreversible heat engine is due to finite rate heat transfer between the working fluid and the reservoirs. Let the total entropy generation rate of the heat engine be σ, one has

$$\sigma = \frac{q_2}{T_2} - \frac{q_1}{T_1} = \frac{q_1}{T_2}\left(\frac{T_{2'}}{T_{1'}} - \frac{T_2}{T_1}\right) = \frac{q_1}{T_2}(\eta_C - \eta) \tag{7}$$

According to Refs. [7, 11, 19, 20, 34-41, 43-44, 46], a variable $T' \equiv T_2 T_{1'}/T_{2'}$ is defined. Eq. (6) further gives $\eta = 1 - T_2/T'$, and the efficiency of the reversible heat engine, i.e. the Carnot efficiency, is given by $\eta_C = 1 - T_2/T_1$ under the same conditions. The formula of η is very similar to that of η_C, so the variable T' is called the Carnot temperature in Refs. [7, 11, 19, 20, 34-41, 43, 44, 46]. Substituting $T_{2'} \equiv T_2 T_{1'}/T'$ into Eq. (4) yields

$$T_{1'} = \left[T_1^n - \frac{T_1^n - T'^n}{(k_1 T_1^3)(T'/T_1)^{n-1}/(k_2 T_2^3) + 1}\right]^{1/n} \tag{8}$$

From $T_{2'} \equiv T_2 T_{1'}/T'$, one further obtains the temperature $T_{2'}$ of the working fluid corresponding to the low-temperature side as follows

$$T_{2'} = \left[\left(\frac{T_1 T_2}{T'}\right)^n - \frac{[(T_1/T')^n - 1]T_2^n}{(k_1 T_1^3)(T'/T_1)^{n-1}/(k_2 T_2^3) + 1}\right]^{1/n} \tag{9}$$

Substituting Eq. (8) into Eq. (3) yields the heat flux rate q_1

$$q_1 = \frac{(5-n)k_1 T_1^{4-n}(T_1^n - T'^n)}{(k_1 T_1^3)(T'/T_1)^{n-1}/(k_2 T_2^3) + 1} \tag{10}$$

Substituting $\eta = 1 - T_2/T'$ and Eq. (10) into Eq. (5) yields

$$P = \frac{(5-n)k_1 T_1^{4-n}(T_1^n - T'^n)}{(k_1 T_1^3)(T'/T_1)^{n-1}/(k_2 T_2^3) + 1}\left(1 - \frac{T_2}{T'}\right) \tag{11}$$

The total entropy generation rate σ is obtained by substituting Eq. (11) into Eq. (7), which is given by

$$\sigma = \frac{(5-n)k_1 T_1^{4-n}(T_1^n - T'^n)}{(k_1 T_1^3)(T'/T_1)^{n-1}/(k_2 T_2^3)+1}\left(\frac{1}{T'}-\frac{1}{T_1}\right) \tag{12}$$

From Eqs. (8)- (12), all of parameters of the heat engine can be expressed as functions of the Carnot temperature T'. If the optimal T' is obtained, the other optimal parameters of the heat engine can also be obtained from T'. Therefore, the optimization problem is simplified by choosing the Carnot temperature T' as the control variable.

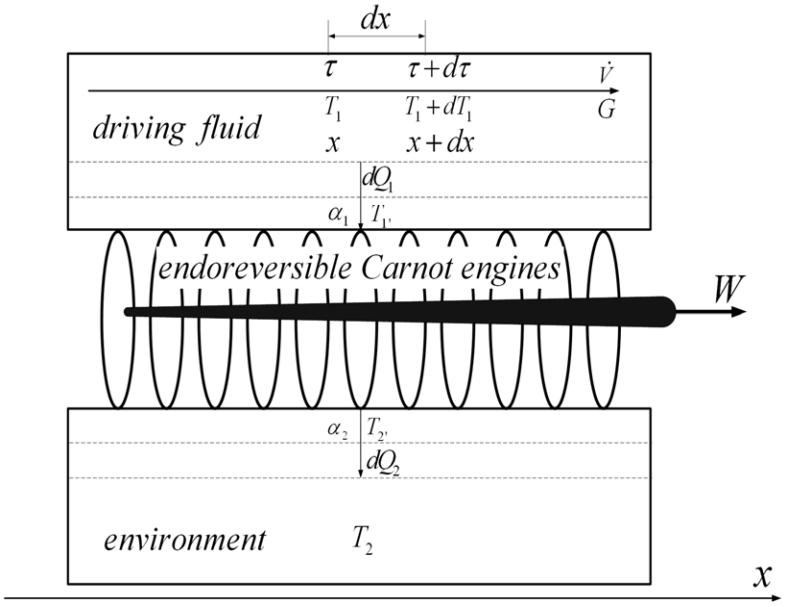

Figure 1. Model of a multistage continuous endoreversible Carnot heat engine system

2.2 The fundamental parameter relationships of a multistage continuous endoreversible Carnot heat engine system

For a multistage continuous endoreversible Carnot heat engine system as shown in Figure 1, the driving fluid at the high-temperature side is black photon flux. G is its molar flux rate, $\dot{V}$ is its volume flux rate, C_V is its molar constant volume heat capacity, and C_h is its substitutional heat capacity. According to the theory of thermodynamics of radiation [31-35, 41-45], the molar volume V_m, molar constant volume heat capacity C_V and molar substitutional heat capacity are, respectively, given by

$$V_m = 3k_B A_v c/(4\sigma_B T^3), \qquad C_V = 12k_B A_v = 12R, \qquad C_h = 16k_B A_v = 16R \tag{13}$$

where k_B is Boltzmann constant, A_v is Avogadro's number, c is the velocity of light, σ_B is Stefan-Boltzmann constant, and R is the universal gas constant. Then the molar flux rate G of the driving fluid is given by

$$G = \dot{V}/V_m = 4\dot{V}\sigma_B T_1^3/(3k_B A_v c) \tag{14}$$

The molar heat capacity rates GC_V and GC_h of the photon flux are obtained by combining Eq. (13) with Eq. (14), which are, respectively, given by

$$GC_V = 16\dot{V}\sigma_B T_1^3/c, \qquad GC_h = 64\dot{V}\sigma_B T_1^3/(3c) \tag{15}$$

Let α_1 and α_2 be the heat transfer coefficients corresponding to the high- and low-temperature sides, respectively, a_{V1} is the heat transfer area between the driving fluid per unit volume and the working fluid of the heat engine at the high-temperature side, and F_1 is the driving fluid cross-sectional area, perpendicular to x. The above parameters are all known for the real systems. For the radiative heat transfer law, one has $\alpha_1 = \sigma_B \varepsilon_1$, where ε_1 is the emissivity of the photon flux. The first law of thermodynamics gives

$$\frac{q_1}{k_1} = \frac{-GC_h dT_1}{\alpha_1 a_{V1} F_1 v dt} = \frac{-GC_h dT_1}{\sigma_B a_{V1} \varepsilon_1 \dot{V} dt} = -\frac{64T_1^3}{3c\varepsilon_1 a_{V1}} \frac{dT_1}{dt} \tag{16}$$

For the given integration section $[\tau_i, \tau_f]$, the boundary temperatures of the driving fluid are denoted as $T_1(\tau_i) = T_{1i}$ and $T_1(\tau_f) = T_{1f}$, then the power output $\dot{W}$ and the entropy generation rate σ_s are, respectively, given by

$$\dot{W}^I = -\int_{T_{1i}}^{T_{1f}} GC_h \eta dT_1 = -\int_{T_{1i}}^{T_{1f}} [\frac{64\dot{V}\sigma_B T_1^3}{3c}(1-\frac{T_2}{T'})]dT_1 = -\int_{t_i}^{t_f} [\frac{64\dot{V}\sigma_B T_1^3}{3c}(1-\frac{T_2}{T'})]\dot{T}_1 dt \tag{17}$$

$$\sigma_s^I = -\int_{T_{1i}}^{T_{1f}} GC_h (\frac{1}{T'} - \frac{1}{T_1})dT_1 = -\int_{T_{1i}}^{T_{1f}} \frac{GC_h}{T_2}(\eta_C - \eta)dT_1 = -\int_{t_i}^{t_f} [\frac{64\dot{V}\sigma_B T_1^3}{3c}(\frac{1}{T'} - \frac{1}{T_1})\dot{T}_1]dt \tag{18}$$

where $\dot{T}_1 = dT_1 / d\tau$. The dot notation signifies the time derivative. The pressure p of the photon flux is a function of the temperature T_1, which is given by $p = 4\sigma_B T_1^4 / (3c)$ according to the thermodynamics of radiation. When effects of change of pressure p on the power output of the multistage heat engine system are considered, another calculation expression of the power output $\dot{W}$ is given by [35-40]

$$\begin{aligned} \dot{W}^{II} &= -\int_{T_{1i}}^{T_{1f}} G[C_V(1-\frac{T_2}{T'}) + \frac{dp}{dT_1}]dT_1 \\ &= -\dot{V}\sigma_B \int_{T_{1i}}^{T_{1f}} [\frac{16T_1^3}{c}(1-\frac{T_2}{T'}) + \frac{16T_1^3}{3c}]dT_1 = -\dot{V}\sigma_B \int_{t_i}^{t_f} (\frac{64T_1^3}{3c} - \frac{16T_1^3}{c}\frac{T_2}{T'})\dot{T}_1 dt \end{aligned} \tag{19}$$

$$\sigma_s^{II} = -\int_{T_{1i}}^{T_{1f}} GC_V (\frac{1}{T'} - \frac{1}{T_1})dT_1 = -\int_{t_i}^{t_f} [\frac{16\dot{V}\sigma_B T_1^3}{c}(\frac{1}{T'} - \frac{1}{T_1})\dot{T}_1]dt \tag{20}$$

Refs. [35-40] calculated the maximum power output for the case with pseudo-Newtonian heat transfer law based on Eq. (19). This paper will further considered two different cases with and without effects of the pressure, and calculate the optimization results for radiative and pseudo-Newtonian heat transfer laws. If the multistage endoreversible Carnot heat engine turns to reversible, Eqs. (17) and (19) further give

$$\dot{W}_{rev}^I = \frac{16\dot{V}\sigma_B(T_{1i}^4 - T_{1f}^4)}{3c} - \frac{64\dot{V}\sigma_B T_2(T_{1i}^3 - T_{1f}^3)}{9c} \tag{21}$$

$$\dot{W}_{rev}^{II} = \frac{16\dot{V}\sigma_B(T_{1i}^4 - T_{1f}^4)}{3c} - \frac{16\dot{V}\sigma_B T_2(T_{1i}^3 - T_{1f}^3)}{3c} \tag{22}$$

In Eqs. (21) and (22), $\dot{W}_{rev}$ is the reversible power output performance limit. If $T_{1f} = T_2$ further, Eqs. (21) and (22), respectively, become

$$\dot{W}_{rev}^{I}=\frac{16\dot{V}\sigma_B T_{1i}^4}{3c}[1-\frac{4}{3}\frac{T_2}{T_{1i}}+\frac{4}{3}(\frac{T_2}{T_{1i}})^4]=\frac{16\dot{V}\sigma_B T_{1i}^4}{3c}\eta_{\mathrm{P}} \tag{23}$$

$$\dot{W}_{rev}^{II}=A_{class}=\frac{16\dot{V}\sigma_B T_{1i}^4}{3c}(1-\frac{T_2}{T_{1i}})=\frac{16\dot{V}\sigma_B T_{1i}^4}{3c}\eta_{\mathrm{j}} \tag{24}$$

η_{P} and η_C in Eqs. (23) and (24) are the named Petela's efficiency and Jeter's efficiency [47-51]. What should be paid attention is that the form of the efficiency η_{j} derived by Jeter is the same as that of Carnot efficiency. A_{class} in Eq. (24) is called classical thermodynamic exergy of radiation photon flux. For the endoreversible Carnot heat engine system considered herein, there exists loss of irreversibility due to the finite rate heat transfer, and the high-temperature driving fluid temperature can not decrease to the low-temperature environment temperature T_2 in a finite time, so the maximum value of Eq. (19) is smaller than A_{class} of Eq. (24) consequentially. Combining Eq. (10) with Eq. (16) yields

$$\frac{dT_1}{dt}=-\frac{\beta(5-n)T_1^{4-n}(T_1^n-T^{'n})}{T_1^3[(k_1T_1^3)(T^{'}/T_1)^{n-1}/(k_2T_2^3)+1]} \tag{25}$$

where $\beta=3c\varepsilon_1 a_{V1}/64$. Substituting Eq. (25) into Eqs. (17) and (19) yields

$$\dot{W}^{I}=\int_{t_i}^{t_f}\{\frac{64\dot{V}\sigma_B\beta(5-n)T_1^{4-n}(T_1^n-T^{'n})}{3c[(k_1T_1^3)(T^{'}/T_1)^{n-1}/(k_2T_2^3)+1]}(1-\frac{T_2}{T^{'}})\}dt \tag{26}$$

$$\dot{W}^{II}=\int_{t_i}^{t_f}\{(\frac{64}{3c}-\frac{16}{c}\frac{T_2}{T^{'}})\frac{\dot{V}\sigma_B\beta(5-n)T_1^{4-n}(T_1^n-T^{'n})}{[(k_1T_1^3)(T^{'}/T_1)^{n-1}/(k_2T_2^3)+1]}\}dt \tag{27}$$

3. Optimization

The problem now is to determine the maximum values of Eqs. (26) and (27) subject to the constraint of Eq. (25). The control variable is $T^{'}\equiv T_2T_{1'}/T_{2'}$, and the inequality $T_1>T_{1'}>T_{2'}>T_2$ always holds for the heat engine, so one obtains $T_2\le T^{'}\le T_1$. This optimal control problem belongs to a variational problem whose control variable has the constraint of closed set, and the Pontryagin's minimum value principle or Bellman's dynamic programming theory may be applied. When the state vector dimension of the optimal control problem is small, the numerical optimization conducted by the dynamic programming theory is very efficient. Let the optimal performance objective of the problem be $\dot{W}_{\max}(T_{1i},\tau_i,T_{1f},\tau_f)$, and the admissible control set of the control variable $T^{'}(t)$ is denoted as Ω. The performance objective of the control problem can be expressed as follows

$$\dot{W}_{\max}(T_{1i},t_i,T_{1f},t_f)\equiv\max_{T^{'}(t)\in\Omega}[\dot{W}(T_{1i},t_i,T_{1f},t_f)]=\max_{T^{'}(t)\in\Omega}[\int_{t_i}^{t_f}f_0(T_1,T^{'},t)dt] \tag{28}$$

The Hamilton-Jacobi-Bellman (HJB) control equation of the optimization problem is

$$\frac{\partial\dot{W}_{\max}}{\partial t}+\max_{T^{'}(t)\in\Omega}\{f_0(T_1,T^{'},t)+\frac{\partial\dot{W}_{\max}}{\partial T_1}f(T_1,T^{'},t)\}=0 \tag{29}$$

where $f_0(T_1,T^{'},t)$ corresponds to integrands in Eqs. (26) and (27), and $f(T_1,T^{'},t)$ corresponds to the right term of Eq. (25). Then HJB control equations corresponding to objectives of Eqs. (26) and (27) are, respectively, given by

$$\frac{\partial \dot{W}_{\max}^{I}}{\partial t}+\max_{T^{'}(t)\in\Omega}\{[GC_h(1-\frac{T_2}{T^{'}})-\frac{\partial W_{\max}^{I}}{\partial T_1}]\frac{\beta(5-n)T_1^{4-n}(T_1^n-T^{'n})}{T_1^3[(k_1T_1^3)(T^{'}/T_1)^{n-1}/(k_2T_2^3)+1]}\}=0 \tag{30}$$

$$\frac{\partial \dot{W}_{\max}^{II}}{\partial t}+\max_{T^{'}(t)\in\Omega}\{[(GC_h-GC_V\frac{T_2}{T^{'}})-\frac{\partial W_{\max}^{II}}{\partial T_1}]\frac{\beta(5-n)T_1^{4-n}(T_1^n-T^{'n})}{T_1^3[(k_1T_1^3)(T^{'}/T_1)^{n-1}/(k_2T_2^3)+1]}\}=0 \tag{31}$$

There are only analytical solutions of Eqs. (30) and (31) for the special cases, while for the radiative heat transfer law, one has to refer to numerical methods. Consider that the continuous differential equation should be discretized for the numerical calculation performed on the computer, and then the discrete equations are given based on Eqs. (25)-(27), as follows

$$(\dot{W}^{I})^{N}=\sum_{i=1}^{N}\{\frac{64\dot{V}\sigma_B\beta\theta^i(5-n)T_1^{4-n}[(T_1^i)^n-(T^{'i})^n]}{3c[k_1(T_1^i)^3(T^{'i}/T_1^i)^{n-1}/(k_2T_2^3)+1]}(1-\frac{T_2}{T^{'i}})\} \tag{32}$$

$$(\dot{W}^{II})^{N}=\sum_{i=1}^{N}\{(\frac{64}{3c}-\frac{16}{c}\frac{T_2}{T^{'i}})\frac{\dot{V}\sigma_B\beta\theta^i(5-n)(T_1^i)^{4-n}[(T_1^i)^n-(T^{'i})^n]}{[k_1(T_1^i)^3(T^{'i}/T_1^i)^{n-1}/(k_2T_2^3)+1]}\} \tag{33}$$

$$T_1^i-T_1^{i-1}=-\frac{\beta(5-n)T_1^{4-n}[(T_1^i)^n-(T^{'i})^n]}{(T_1^i)^3[k_1(T_1^i)^3(T^{'i}/T_1^i)^{n-1}/(k_2T_2^3)+1]}\theta^i \tag{34}$$

$$t^i-t^{i-1}=\theta^i \tag{35}$$

The optimal control problem is to determine the maximum values of Eqs. (32) and (33) subject to the constraints of discrete Eqs. (34) and (35). From Eqs. (32)-(35), the Bellman's backward recurrence equations corresponding to Eqs. (32) and (33) are, respectively, given by

$$\begin{aligned}\dot{W}_{\max}^{(I)i}(T_1^i,t^i)=\max_{T^{'i},\theta^i}\{&\frac{64\dot{V}\sigma_B\beta\theta^i(5-n)T_1^{4-n}[(T_1^i)^n-(T^{'i})^n]}{3c[k_1(T_1^i)^3(T^{'i}/T_1^i)^{n-1}/(k_2T_2^3)+1]}(1-\frac{T_2}{T^{'i}})\\&+\dot{W}_{\max}^{(I)i-1}(T_1^i+\theta^i\frac{\beta(5-n)T_1^{4-n}[(T_1^i)^n-(T^{'i})^n]}{(T_1^i)^3[k_1(T_1^i)^3(T^{'i}/T_1^i)^{n-1}/(k_2T_2^3)+1]},t^i-\theta^i)\}\end{aligned} \tag{36}$$

$$\begin{aligned}\dot{W}_{\max}^{(II)i}(T_1^i,t^i)=\max_{T^{'i},\theta^i}\{&(\frac{64}{3c}-\frac{16}{c}\frac{T_2}{T^{'i}})\frac{\dot{V}\sigma_B\beta\theta^i(5-n)(T_1^i)^{4-n}[(T_1^i)^n-(T^{'i})^n]}{[k_1(T_1^i)^3(T^{'i}/T_1^i)^{n-1}/(k_2T_2^3)+1]}\\&+\dot{W}_{\max}^{(II)i-1}(T_1^i+\theta^i\frac{\beta(5-n)T_1^{4-n}[(T_1^i)^n-(T^{'i})^n]}{(T_1^i)^3[k_1(T_1^i)^3(T^{'i}/T_1^i)^{n-1}/(k_2T_2^3)+1]},t^i-\theta^i)\}\end{aligned} \tag{37}$$

4. Analysis for special cases

4.1 For pseudo-Newtonian heat transfer law

When $n=1$, i.e. the heat transfer between the working fluid and the heat reservoir obeys pseudo-Newtonian heat transfer law. From Appendix A, Refs. [11, 35-40] derived analytical solutions of extremum power output and the optimal fluid temperature configuration based on pseudo-Newtonian heat transfer law, i.e. Eqs. (A12) and (A14). However, Eqs. (A12) and (A14) were obtained based on the condition that the total equivalent thermal conductance is a constant. This condition is very strictly, which is due to that the total equivalent thermal conductance is a function of the reservoir temperature T_1. The temperature T_1 changes along the fluid flow direction, so the condition that the total thermal conductance is a constant is difficult to hold. Thus there are also no analytical solutions for the case with the pseudo-Newtonian heat transfer law, but some algebra equations related to the optimal solutions can be obtained. Eqs. (25), (30) and (31), respectively, become

$$\frac{dT_1}{dt}=-\frac{4\beta(T_1-T^{'})}{[(k_1T_1^3)/(k_2T_2^3)+1]} \tag{38}$$

$$\frac{\partial \dot{W}_{\max}^{I}}{\partial t}+\max_{T^{'}(t)\in\Omega}\{[GC_h(1-\frac{T_2}{T^{'}})-\frac{\partial W_{\max}^{I}}{\partial T_1}]\frac{4\beta(T_1-T^{'})}{[(k_1T_1^3)/(k_2T_2^3)+1]}\}=0 \tag{39}$$

$$\frac{\partial \dot{W}_{\max}^{II}}{\partial t}+\max_{T^{'}(t)\in\Omega}\{[(GC_h-GC_V\frac{T_2}{T^{'}})-\frac{\partial W_{\max}^{II}}{\partial T_1}]\frac{4\beta(T_1-T^{'})}{[(k_1T_1^3)/(k_2T_2^3)+1]}\}=0 \tag{40}$$

When $W_{\max}^{I}$ is chosen to be the optimization objective, maximizing the second term of Eq. (39) with respect to $T^{'}$ yields

$$T^{'}=\sqrt{T_1T_2/[1-(GC_h)^{-1}(\partial \dot{W}_{\max}^{I}/\partial T_1)/]} \tag{41}$$

Substituting Eq. (41) into Eq. (39) yields

$$\frac{\partial \dot{W}_{\max}^{I}}{\partial t}+\frac{4\beta GC_hT_1}{[(k_1T_1^3)/(k_2T_2^3)+1]}\{\sqrt{[1-(GC_h)^{-1}(\partial \dot{W}_{\max}^{I}/\partial T_1)]}-\sqrt{T_2/T_1}\}^2=0 \tag{42}$$

The second term of Eq. (42) is the extremum Hamilton function $H(T_1,\partial \dot{W}_{\max}^{I}/\partial T_1)$

$$H(T_1,\partial \dot{W}_{\max}^{I}/\partial T_1)=\frac{4\beta GC_hT_1}{[(k_1T_1^3)/(k_2T_2^3)+1]}\{\sqrt{[1-(GC_h)^{-1}(\partial \dot{W}_{\max}^{I}/\partial T_1)]}-\sqrt{T_2/T_1}\}^2 \tag{43}$$

From Eq. (43), one can see that H contains the variable τ inexplicitly, and the equation $dH/d\tau=\partial H/\partial\tau$ holds for the Hamilton function, so the Hamilton function is autonomous and $H(T_1,\partial \dot{W}_{\max}^{I}/\partial T_1)$ keeps constant along the optimal path. Let the constant be h, and one further obtains

$$\frac{4\beta GC_hT_1}{[(k_1T_1^3)/(k_2T_2^3)+1]}\{\sqrt{[1-(GC_h)^{-1}(\partial \dot{W}_{\max}^{I}/\partial T_1)]}-\sqrt{T_2/T_1}\}^2=h \tag{44}$$

From Eq. (44), one obtains $\partial \dot{W}_{\max}^{I}/\partial T_1$, as follows

$$\partial \dot{W}_{\max}^{I}/\partial T_1=GC_h\{1-\{\sqrt{h[(k_1T_1^3)/(k_2T_2^3)+1]/(4GC_h\beta T_1)}+\sqrt{T_2/T_1}\}^2\} \tag{45}$$

Substituting Eq. (45) into Eq. (41) yields

$$T^{'}=T_1/\{\sqrt{h[(k_1T_1^3)/(k_2T_2^3)+1]/(4GC_h\beta T_2)}+1\} \tag{46}$$

Substituting Eq. (46) into Eq. (38) yields

$$\frac{dT_1}{dt}=-\frac{4\beta T_1\sqrt{h[(k_1T_1^3)/(k_2T_2^3)+1]/(4GC_h\beta T_2)}}{[(k_1T_1^3)/(k_2T_2^3)+1][\sqrt{h[(k_1T_1^3)/(k_2T_2^3)+1]/(4GC_h\beta T_2)}+1]} \tag{47}$$

For the given boundary conditions $T_1(t_i)=T_{1i}$ and $T_1(t_f)=T_{1f}$, an equation related to the Hamiltonian constant h is obtained by substituting $GC_h=64\dot{V}\sigma_BT_1^3/(3c)$ into Eq. (47)

$$\frac{k_1}{12k_2\beta T_2^3}(T_{1f}^3-T_{1i}^3)+\frac{1}{4\beta}\ln(T_{1f}/T_{1i})+\int_{T_{1i}}^{T_{1f}}\{\frac{4\sqrt{\dot{V}\sigma_BT_1T_2[(k_1T_1^3)/(k_2T_2^3)+1]}}{\sqrt{3\beta ch}}\}dT_1=t_i-t_f \tag{48}$$

The Hamiltonian constant h corresponding to the objective $\dot{W}^{I}_{\max}$ is obtained from Eq. (48), and then substituting h into Eq. (47). Eq. (47) becomes the problem of initial value of differential equation, and the optimal temperature T_1 versus the time t is obtained.

When $W^{II}_{\max}$ is chosen to be optimization objective and though some mathematical derivations, the similar equations to Eqs. (47) and (48) are also obtained, which are, respectively, given by

$$\frac{dT_1}{dt}=-\frac{4\beta T_1\sqrt{h[(k_1T_1^3)/(k_2T_2^3)+1]/(4GC_V\beta T_2)}}{[(k_1T_1^3)/(k_2T_2^3)+1]\{\sqrt{h[(k_1T_1^3)/(k_2T_2^3)+1]/(4GC_V\beta T_2)}+1\}} \tag{49}$$

$$\frac{k_1(T_{1f}^3-T_{1i}^3)}{12k_2\beta T_2^3}+\frac{1}{4\beta}\ln(T_{1f}/T_{1i})+\int_{T_{1i}}^{T_{1f}}\{\frac{2\sqrt{\dot{V}\sigma_B T_1T_2[(k_1T_1^3)/(k_2T_2^3)+1]}}{\sqrt{\beta ch}}\}dT_1=t_i-t_f \tag{50}$$

For the given boundary conditions $T_1(t_i)=T_{1i}$ and $T_1(t_f)=T_{1f}$, the Hamiltonian constant h corresponding to the objective $\dot{W}^{I}_{\max}$ is obtained from Eq. (50). And then substituting h into Eq. (49), and Eq. (49) becomes the problem of initial value of differential equation, so the optimal temperature T_1 versus the time t is also obtained.

What should be paid attention is that the above methods are only suitable for the case with the fixed final driving fluid temperature T_{1f}. While for the case with the free T_{1f}, one has to refer to dynamic programming algorithm (Figure 2).

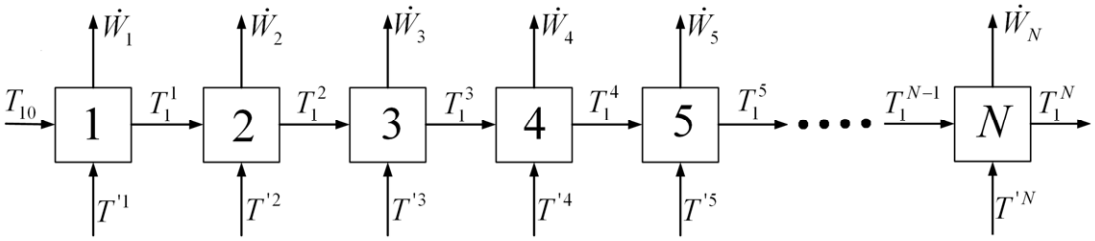

Figure 2. The dynamic programming schematic plan of the multistage discrete endoreversible Carnot heat engines [36]

4.2 For Stefan-Boltzmann heat transfer law

When $n=4$, i.e. the heat transfer between the working fluid and the heat reservoir obeys Stefan-Boltzmann heat transfer law. Eqs. (25), (30) and (31), respectively, become

$$\frac{dT_1}{dt}=-\frac{\beta(T_1^4-T'^4)}{T_1^3[(k_1/k_2)(T'/T_2)^3+1]} \tag{51}$$

$$\frac{\partial\dot{W}^{I}_{\max}}{\partial t}+\max_{T'(t)\in\Omega}\{[\frac{64\dot{V}\sigma_B T_1^3}{3c}(1-\frac{T_2}{T'})-\frac{\partial W^{I}_{\max}}{\partial T_1}]\frac{\beta(T_1^4-T'^4)}{T_1^3[(k_1/k_2)(T'/T_1)^3+1]}\}=0 \tag{52}$$

$$\frac{\partial\dot{W}^{II}_{\max}}{\partial t}+\max_{T'(t)\in\Omega}\{[(\frac{64\dot{V}\sigma_B T_1^3}{3c}-\frac{16\dot{V}\sigma_B T_1^3}{c}\frac{T_2}{T'})-\frac{\partial W^{II}_{\max}}{\partial T_1}]\frac{\beta(T_1^4-T'^4)}{T_1^3[(k_1/k_2)(T'/T_1)^3+1]}\}=0 \tag{53}$$

There are no analytical solutions of Eqs. (51)-(53) for the radiative heat transfer law, and one has refer to numerical methods. For numerical calculations, Eqs. (32)-(34), respectively, become

$$(\dot{W}^{I})^{N}=\sum_{i=1}^{N}\{\frac{64\dot{V}\sigma_B\beta\theta^i[(T_1^i)^4-(T'^i)^4]}{3c[(k_1/k_2)(T'^i/T_2)^3+1]}(1-\frac{T_2}{T'^i})\} \tag{54}$$

$$(\dot{W}^{II})^N = \sum_{i=1}^{N}\{(\frac{64}{3c} - \frac{16}{c}\frac{T_2}{T^{'i}})\frac{\dot{V}\sigma_B\beta\theta^i[(T_1^i)^4 - (T^{'i})^4]}{[(k_1/k_2)(T^{'i}/T_2)^3 + 1]}\} \tag{55}$$

$$T_1^i - T_1^{i-1} = -\frac{\beta[(T_1^i)^4 - (T^{'i})^4]}{(T_1^i)^3[(k_1/k_2)(T^{'i}/T_1^i)^3 + 1]}\theta^i \tag{56}$$

The Bellman's backward recurrence equations corresponding to the objective functions $\dot{W}^I$ and $\dot{W}^{II}$ are, respectively, given by

$$\begin{aligned}\dot{W}_{\max}^{(I)i}(T_1^i, \tau^i) = \max_{T^{'i},\theta^i}\{&\frac{64\dot{V}\sigma_B\beta\theta^i[(T_1^i)^4 - (T^{'i})^4]}{3c[(k_1/k_2)(T^{'i}/T_2)^3 + 1]}(1 - \frac{T_2}{T^{'i}}) \\ &+ \dot{W}_{\max}^{(I)i-1}(T_1^i + \theta^i\frac{\beta[(T_1^i)^4 - (T^{'i})^4]}{(T_1^i)^3[(k_1/k_2)(T^{'i}/T_2)^3 + 1]}, t^i - \theta^i)\}\end{aligned} \tag{57}$$

$$\begin{aligned}\dot{W}_{\max}^{(II)i}(T_1^i, \tau^i) = \max_{T^{'i},\theta^i}\{&(\frac{64}{3c} - \frac{16}{c}\frac{T_2}{T^{'i}})\frac{\dot{V}\sigma_B\beta\theta^i[(T_1^i)^4 - (T^{'i})^4]}{(k_1/k_2)(T^{'i}/T_2)^3 + 1} \\ &+ \dot{W}_{\max}^{(II)i-1}(T_1^i + \theta^i\frac{\beta[(T_1^i)^4 - (T^{'i})^4]}{(T_1^i)^3[(k_1/k_2)(T^{'i}/T_2)^3 + 1]}, t^i - \theta^i)\}\end{aligned} \tag{58}$$

5. Numerical examples and discussions

Refs. [43, 44] show that the maximum power output of the multistage heat engine system is $\dot{W}_{\max} = \dot{W}_{rev} - T_2\sigma_s$. When the total process period is fixed (i.e. the total heat conductance of the driving fluid at the high-temperature side is fixed), the final driving fluid temperature at the high-temperature side can not decrease to the environment temperature, and there is a low limit value $\overline{T}_{1f}$. With the decrease of the final temperature T_{1f}, both the reversible power output $\dot{W}_{rev}$ and the total entropy generation rate σ_s increase, so the relationship between $\dot{W}_{\max}$ and T_{1f} is unknown. Since $\dot{W}_{\max}$ is the continuous function of T_{1f}, there is an optimal T_{1f}^* during the closed section $[\overline{T}_{1f}, T_{1i}]$ for $\dot{W}_{\max}$ to achieve its maximum value. This was ignored in Refs. [5, 7, 11, 13-22, 34-42], which chose the low-temperature environment temperature T_2 as the final temperature. The same analysis methods as Refs. [43, 44] are adopted herein, and numerical solutions for the radiative heat transfer law [$q \propto \Delta(T^4)$] are solved by dynamic programming algorithm [52, 53] by taking the power output $\dot{W}^I$ of the system for example. Two different boundary conditions including fixed and free final temperatures are considered herein, and optimization results for the radiative heat transfer law are compared with those for the pseudo-Newtonian heat transfer law.

According to Refs. [35, 36], the following calculation parameters are set: the volume flow rate of the high-temperature radiation photo flux is $\dot{V} = 10^4 m^3/s$, the initial temperature is $T_{10} = 5800K$, the environment temperature at the low-temperature side is $T_2 = 300K$, the velocity of the light is $c = 2.998\times10^8 m/s$, Stefan-Boltzmann constant is $\sigma_B = 5.66667\times10^{-8} W/(m^2\cdot K^4)$, Avogadro's number is $A_v = 6.0221367\times10^{23}(1/mol)$, Boltzmann constant is $k_B = 1.380658\times10^{-23} J/K$, the universal gas constant is $R = k_B A_v = 8.314510 J/(mol\cdot K)$, the emissivity are $\varepsilon_1 = \varepsilon_2 = 1$. The grid division of the time coordinate is linear. Since $\beta = 3c\varepsilon_1 a_{V1}/64$ and its unit is $1/s$, $\beta\theta^i$ is a dimensionless quantity and $\beta\theta^i = 0.15$ is set herein. Let $k_2 = k_1$ for the radiative heat transfer law, and $k_2 = 100k_1$ for pseudo-Newtonian heat transfer law.

5.1 Performance analysis for a single steady heat engine

Figure 3 shows the heat flux rate q_1 absorbed by the heat engine versus Carnot temperature $T^{'}$ for two different heat transfer laws. From Figure 3, one can see that with the increase of Carnot temperature $T^{'}$, the heat flux rate q_1 for the pseudo-Newtonian heat transfer law decreases linearly, while that for the radiative heat transfer law decreases non-linearly; for the same Carnot temperature $T^{'}$, the heat flux rate

q_1 for the pseudo-Newtonian heat transfer law increases with the increase of the heat conductance at the low-temperature side. Figure 4 shows the efficiency η of the heat engine versus Carnot temperature $T^{'}$. Since $\eta = 1 - T_2 / T^{'}$, η increases with the increase of $T^{'}$, but its relative increase amount decreases, which is independent of heat transfer laws. Figure 5 shows the power P of the heat engine versus Carnot temperature $T^{'}$. From Figure 5, one can see that there is an extremum for P with respect to Carnot temperature $T^{'}$, and the optimal Carnot temperatures $T^{'}$ corresponding to the maximum power output for different heat transfer laws are different from each other; for the same Carnot temperature $T^{'}$, the power P of the heat engine increases with the increase of the heat conductance at the low-temperature side. Figure 6 shows the entropy generation rate σ versus Carnot temperature $T^{'}$. From Figure 6, one can see that the entropy generation rate σ for different heat transfer laws decreases with the increase of Carnot temperature $T^{'}$. Especially when Carnot temperature $T^{'}$ is small, the entropy generation rate decreases fast, and its change rate tends to be smoothly with the increase of Carnot temperature $T^{'}$. From $T^{'} \equiv T_2 T_{1'} / T_{2'}$ and when $T^{'} = T_2 = 300K$, the heat-absorbed temperature $T_{1'}$ of the working fluid in the endoreversible Carnot heat engine is equal to its heat-released temperature $T_{2'}$, i.e. the limit Carnot cycle, the heat flux rate q_1 absorbed by the working fluid is equal to that released, the heat engine efficiency η is equal to zero as shown in Figure 4, the power output P of the heat engine is also equal to zero as shown in Figure 5, and the entropy generation rate achieves its maximum value as shown in Figure 6. While $T^{'} = T_1 = 5800K$, the heat-absorbed temperature $T_{1'}$ of the working fluid in the endoreversible Carnot heat engine is equal to the high-temperature reservoir temperature T_1, and the heat-released temperature of the working fluid is equal to the low-temperature reservoir temperature T_2, i.e. the reversible Carnot cycle. The rate of heat absorbed q_1 is equal to zero as shown in Figure 3, the heat engine efficiency achieve its maximum value and equals to the Carnot efficiency $\eta_C = 1 - T_2 / T_1$ as shown in Figure 4, its power P is equal to zero as shown in Figure 5, and the entropy generation rate σ is also equal to zero as shown in Figure 6.

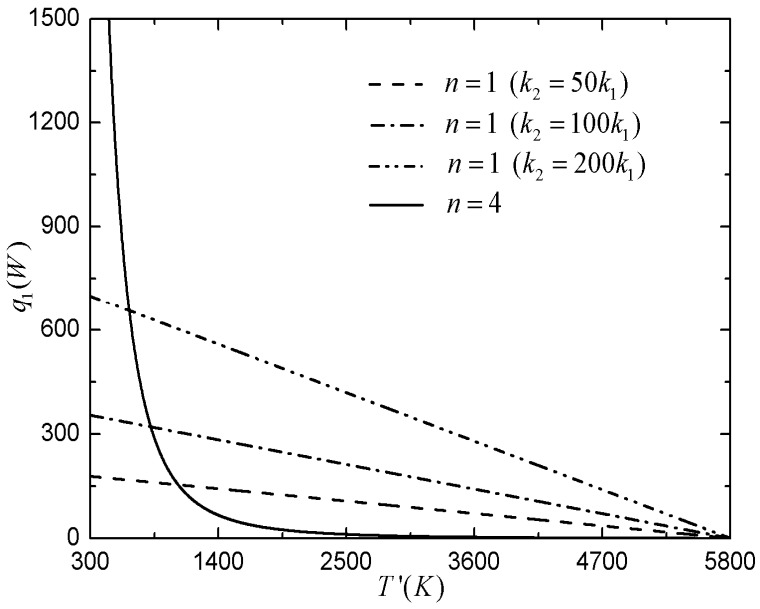

Figure 3. The absorbed heat flux rate q_1 of the single-stage heat engine versus Carnot temperature $T^{'}$

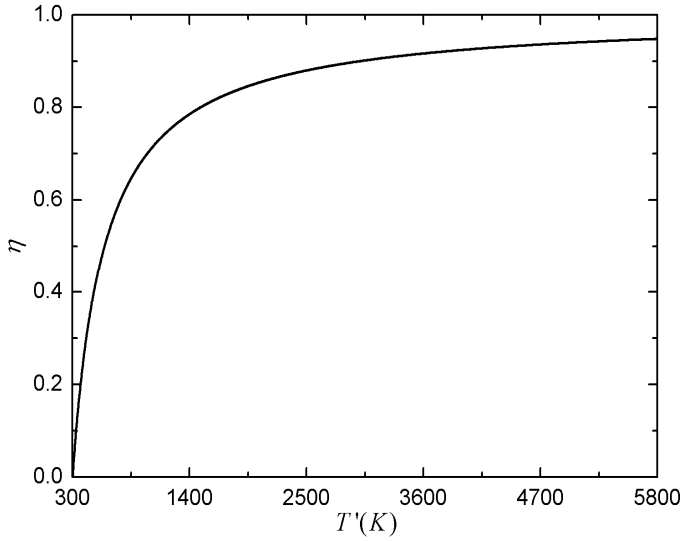

Figure 4. The efficiency η of the single-stage heat engine versus Carnot temperature T'

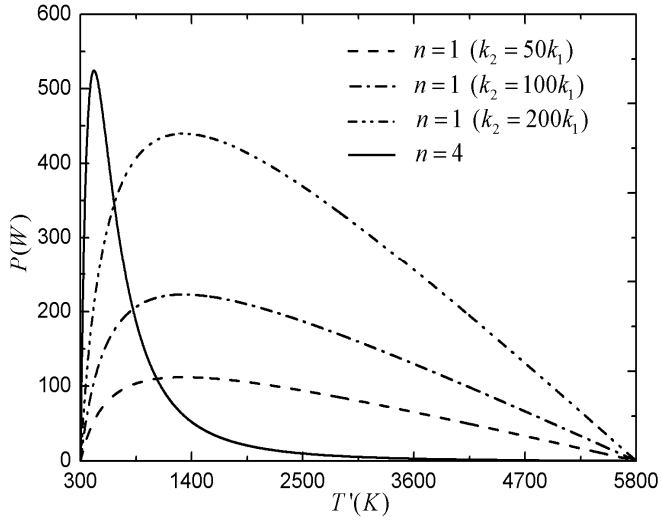

Figure 5. The power output P of the single-stage heat engine versus Carnot temperature T'

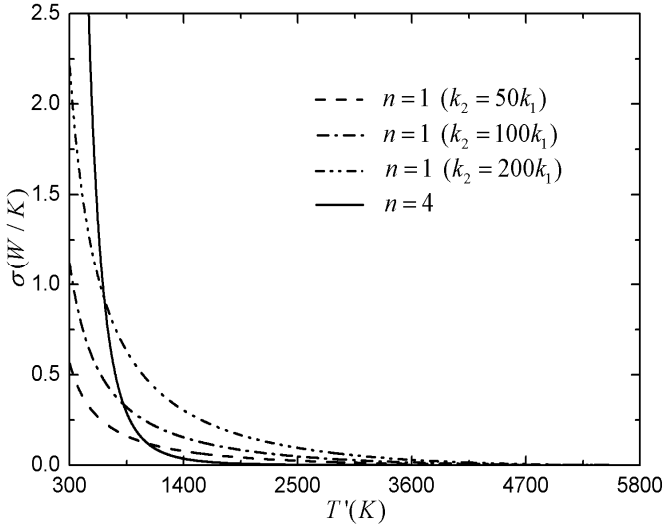

Figure 6. The entropy generation rate σ of the single-stage heat engine versus Carnot temperature T'

5.2 Numerical examples for the multistage heat engine system with the radiative heat transfer law

5.2.1 For the fixed final temperature

When the final temperature T_{1f} is fixed, the reversible power output W_{rev} is also fixed, and then optimization for maximizing power output is equivalent to that for minimizing entropy generation due to $\dot{W} = W_{rev} - T_2\sigma_s$. In order to analyze effects of the final temperature T_{1f} on the optimization results, the final temperature is set to be $T_{1f} = 500K$, $T_{1f} = 1000K$, and $T_{1f} = 1500K$. Figures 7 and 8 show the optimal fluid temperature T_1 and Carnot temperature T' versus the time βt. Figure 9 shows the optimal power output $\dot{W}_i$ of the heat engine versus the stage i. In Figures 7-9, the continuous lines denote the analytical optimization results, while the discrete points denote the numerical optimization results. The total stage $N = 100$ of heat engines are shown with the step of 2 in Figures 7-9. Table 1 lists optimization results of the key parameters of the multistage endoreversible heat engine system with the radiative heat transfer law. From Figure 7, one can see that the driving fluid temperature T_1 decreases non-linearly with the increase of the time βt. From Figures 8 and 9, one can see that when $T_{1f} = 500K$ and $T_{1f} = 1000K$, the optimal Carnot temperature profiles consist of two segments: the heat engines in the former segment have power output, while those in the latter segment have no power output due to $T' = 300K$. What should be paid attention is that the heat engines in the latter segment seem to be shortened so that the fluid temperature at the high-temperature side decreases to the desired final temperature at the fast speed. When $T_{1f} = 1500K$, there is power output for each stage heat engine. From Table 1, one can see that when $T_{1f} = 500K$, one obtains $T'(0) = 981.1K$ and $\dot{W}_{\max} = 6.88 \times 10^3 W$; when $T_{1f} = 1000K$, one obtains $T'(0) = 1020.7K$ and $\dot{W}_{\max} = 7.05 \times 10^3 W$; when $T_{1f} = 1500K$, one obtains $T'(0) = 1040.0K$ and $\dot{W}_{\max} = 7.13 \times 10^3 W$, i.e. both the initial Carnot temperature $T'(0)$ and the maximum power output $\dot{W}_{\max}$ increase with the increase of the final temperature T_{1f}. Both the maximum power output of the multistage heat engine system with the radiative heat transfer law and the corresponding optimal control are different for the cases with different final fluid temperatures. From the above analysis, the boundary temperature change has significant effects on the power output optimization results of the multistage heat engine system.

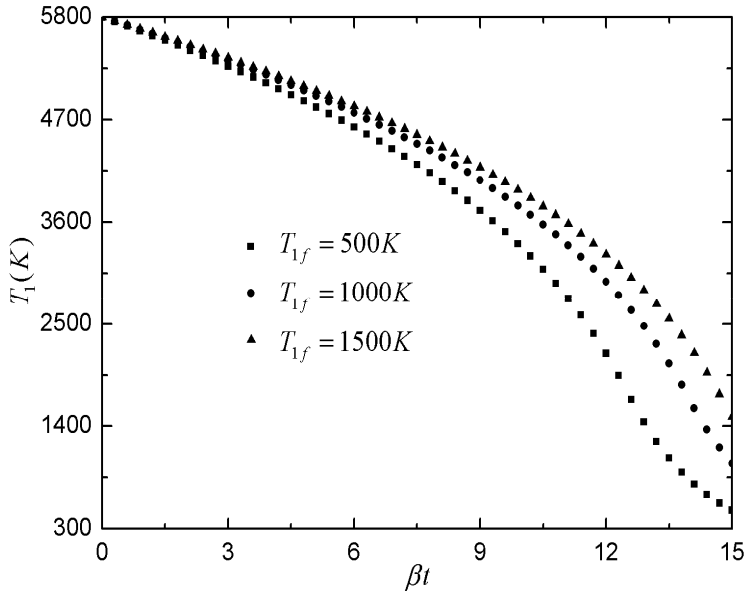

Figure 7. The optimal driving fluid temperature T_1 versus the dimensionless time βt for Newtonian heat transfer law (fixed T_{1f})

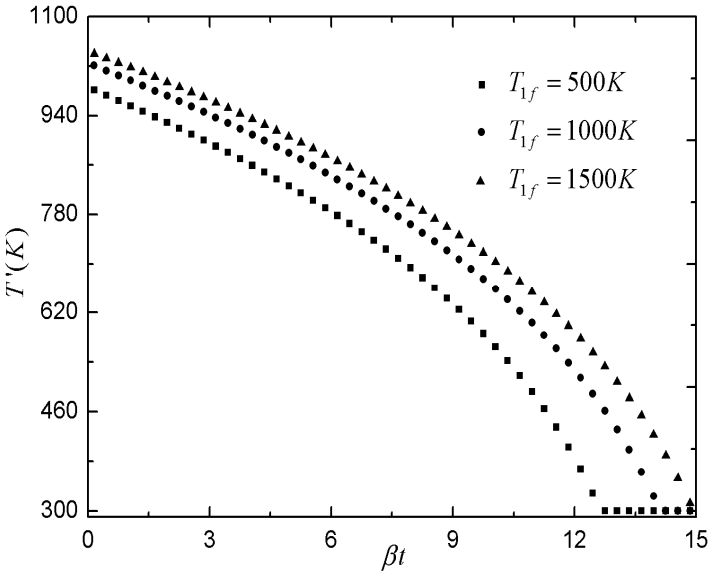

Figure 8. The optimal Carnot temperature T' versus the dimensionless time βt for Newtonian heat transfer law (fixed T_{1f})

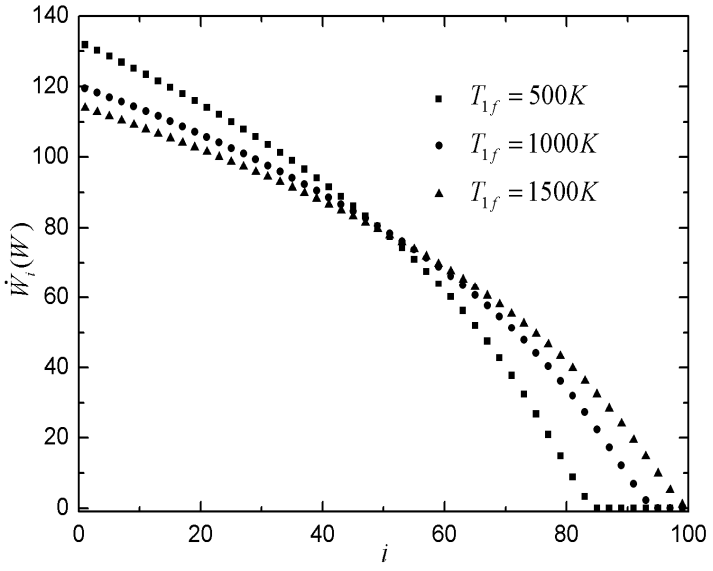

Figure 9. The optimal power output $\dot{W}_i$ of each stage heat engine versus the stage i for Newtonian heat transfer law (fixed T_{1f})

Table 1. Optimization results of the key parameters of the multistage endoreversible heat engine system with the radiative heat transfer law

Fixed T_{1f} ($t_1=150s$)	Key parameters	$T'(0)$		$\dot{W}_{\max}$
	$T_{1f}=500K$	$981.1K$		6.88×10^3W
	$T_{1f}=1000K$	$1020.7K$		7.05×10^3W
	$T_{1f}=1500K$	$1040.0K$		7.13×10^3W
Free T_{1f}	Key parameters	T_{1f}^*	$T'(0)$	$\dot{W}_{\max}^*$
	$\beta\theta^i=0.10$	$2626.9K$	$937.4K$	6.57×10^3W
	$\beta\theta^i=0.15$	$2286.0K$	$1070.2K$	7.19×10^3W
	$\beta\theta^i=0.30$	$1770.6K$	$1346.9K$	8.09×10^3W

5.2.2 For the free final temperature

When the final temperature T_{1f} is free, both the reversible power output W_{rev} and the entropy generation rate σ_s increase with the decrease of the final temperature T_{1f}. When $T_{1f} = T_{1i}$, the minimum entropy generation is equal to zero, and optimization for maximizing power output is not equivalent to that for minimizing entropy generation. In order to analyze effects of change of the total time on the optimization results, the infinitesimal dimensionless time is chosen to be $\beta\theta^i = 0.10$, $\beta\theta^i = 0.15$, and $\beta\theta^i = 0.30$. Figures 10 and 11 show the optimal fluid temperature T_1 and optimal Carnot temperature T' versus the dimensionless time βt, respectively, and Figure 12 shows the corresponding optimal power output $\dot{W}_i$ of each stage heat engine versus the stage i. From Figures 10 and 11, one can see that both the fluid temperature T_1 and Carnot temperature T' decrease nonlinearly with the increase of the time βt;, both the optimal final temperature T_{1f}^* and Carnot temperature T' decrease with the increase of the infinitesimal dimensionless time $\beta\theta^i$. From Table 1, one can see that when $\beta\theta^i = 0.10$, one obtains $T_{1f}^* = 2626.9K$, $T'(0) = 937.4K$ and $\dot{W}_{\max}^* = 6.57\times10^3 W$; when $\beta\theta^i = 0.15$, one obtains $T_{1f}^* = 2286.0K$, $T'(0) = 1070.2K$ and $\dot{W}_{\max}^* = 7.19\times10^3 W$; when $\beta\theta^i = 0.30$, one obtains $T_{1f}^* = 1770.6K$, $T'(0) = 1346.9K$ and $\dot{W}_{\max}^* = 8.09\times10^3 W$, i.e. with the increase of $\beta\theta^i$, the final temperature T_{1f}^* increases, the initial Carnot temperature $T'(0)$ increases, and the maximum power output $\dot{W}_{\max}^*$ of the system increases. From Figure 12, one can see that the power output $\dot{W}_i$ of each stage heat engine decreases with the increase of the stage i, which is due to that the driving fluid temperature T_1 decreases with the increase of the time βt; when the stage i is small, the power output $\dot{W}_i$ increases with the increase of $\beta\theta^i$, while the stage i is relative large, the power output $\dot{W}_i$ decreases with the increase of $\beta\theta^i$, i.e. the optimal distributions of the power output $\dot{W}_i$ along the stage i are different for different total time constraints. This shows that the change of the total time constraint has significant effects on the power output optimization results of the multistage heat engine system.

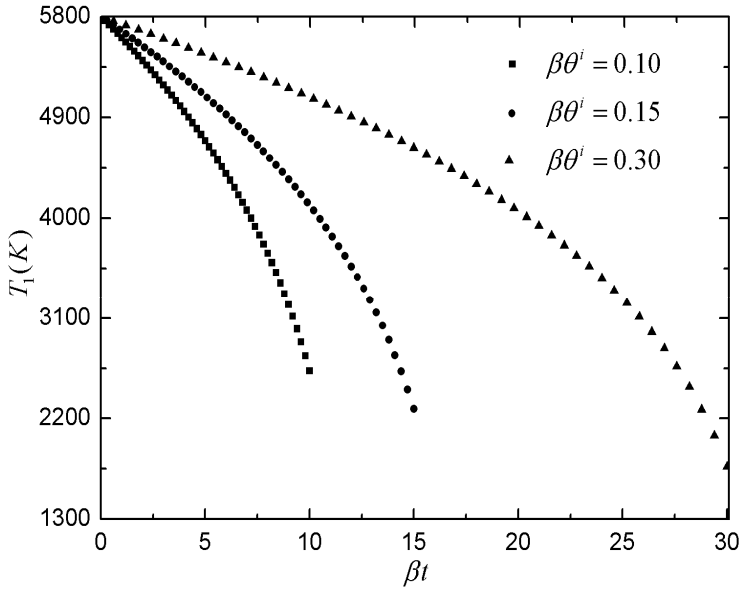

Figure 10. The optimal driving fluid temperature T_1 versus the dimensionless time βt for Newtonian heat transfer law (free T_{1f})

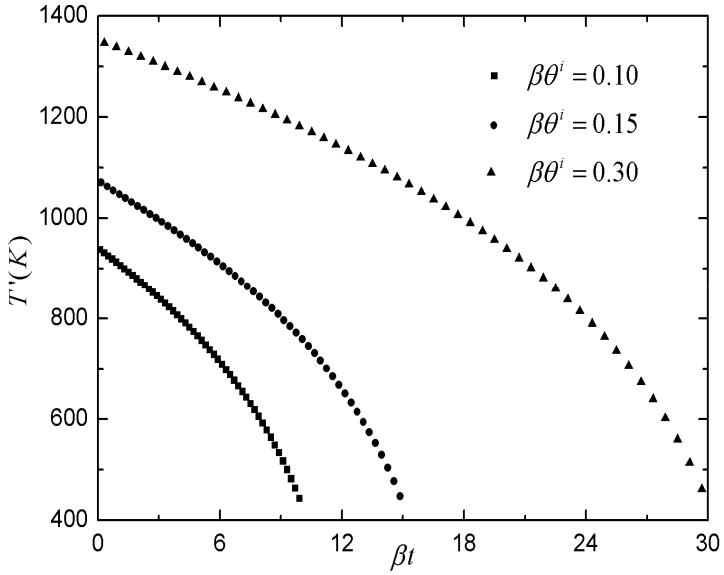

Figure 11. The optimal Carnot temperature T' versus the dimensionless time βt for Newtonian heat transfer law (free T_{1f})

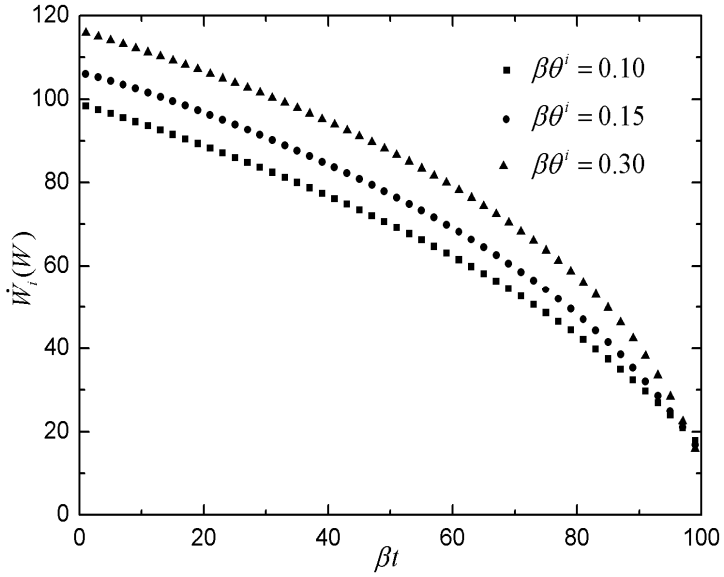

Figure 12. The optimal power output $\dot{W}_i$ of each stage heat engine versus the stage i for Newtonian heat transfer law (free T_{1f})

5.3 Comparison of the optimization results with different heat transfer laws

5.3.1 For the fixed final temperature T_{1f}

When the final temperature is fixed, let $\beta\theta^i = 0.15$ and $T_{1f} = 500K$. Figure 13 shows the optimal fluid temperature T_1 and Carnot temperature T' versus the dimensionless time βt for the fixed final temperature and two different heat transfer laws, and Figure 14 shows the corresponding optimal power output $\dot{W}_i$ of each stage heat engine versus the stage i. From Figure 13, one can see that the fluid temperature for the radiative heat transfer law is lower than that for the pseudo-Newtonian heat transfer law, and the optimal Carnot temperatures for two different heat transfer laws are not equal at the same time. From Figure 14, the power output of each stage heat engine for the radiative heat transfer law is smaller than that for the pseudo-Newtonian heat transfer law. This shows that heat transfer laws have significant effects on the maximum power output of the multistage heat engine system for the fixed final temperature.

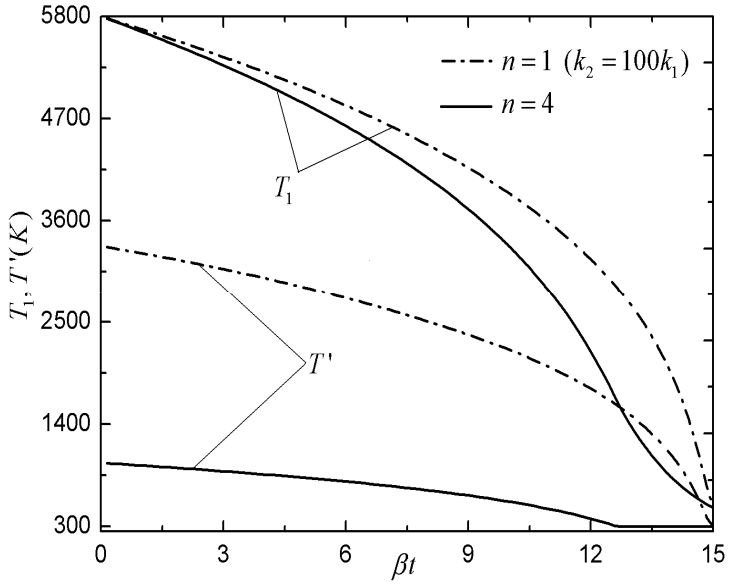

Figure 13. The optimal driving fluid temperature T_1 and optimal Carnot temperature T' versus the dimensionless time βt (fixed T_{1f})

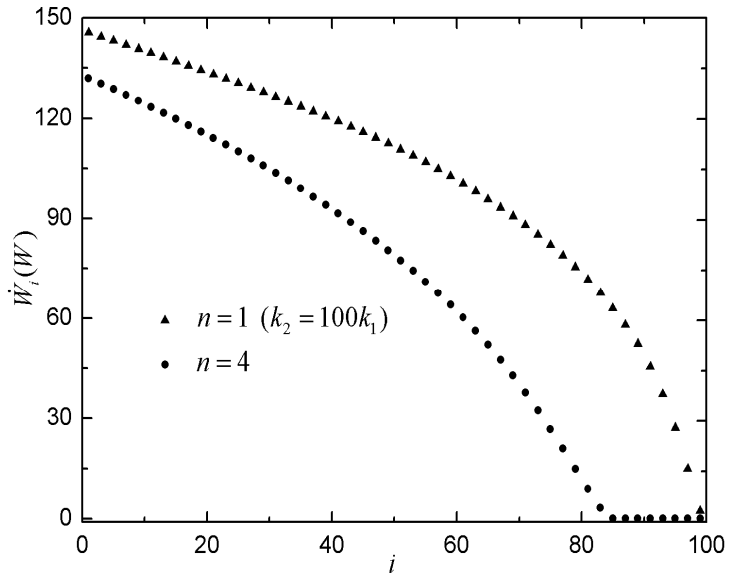

Figure 14. The optimal power output $\dot{W}_i$ of each stage heat engine versus the stage i (fixed T_{1f})

5.3.2 For the free final temperature T_{1f}

When the final temperature is free, let $\beta\theta^i = 0.15$. Figure 15 shows the fluid temperature T_1 and Carnot temperature T' versus the dimensionless time βt for the free final temperature and two different heat transfer laws, which includes the optimization results for the pseudo-Newtonian and radiative heat transfer laws, and stage-by-stage optimization (i.e. the first stage is optimized, and then the second stage is optimized, such-and-such repetition) results for the radiative heat transfer law. Figure 16 shows the corresponding optimal power output of each stage heat engine versus the stage. From Figure 15, one can see that the optimal fluid temperature for the radiative heat transfer law is higher than that for the pseudo-Newtonian heat transfer law, which is contrast to that for the fixed final temperature, but the optimal Carnot temperature for the pseudo-Newtonian heat transfer law is still higher than that for the radiative heat transfer law; the fluid temperature for the stage-by-stage optimization strategy with the radiative heat transfer law decreases fast, and the final temperature is approximate equal to the environment temperature. From Figure 16, one can see that the power output of each stage heat engine for the pseudo-

Newtonian heat transfer law is larger than that for the radiative heat transfer law; the power output of each stage heat engine for the stage-by-stage optimization strategy with the radiative heat transfer law decreases fast with the increase of the stage i, while the power output distribution of each stage heat engine along the stage i for the optimal strategy is relative uniform. Calculation results show that the total power output of the system for the stage-by-stage optimization strategy is $3.71\times10^{3}W$, while that for the global optimization strategy is $7.19\times10^{3}W$, i.e. the total power output after optimization is increased by nearly 93.8%. This shows that both heat transfer laws and boundary condition change have significant effects on the maximum power output of the multistage heat engine system for the free final temperature.

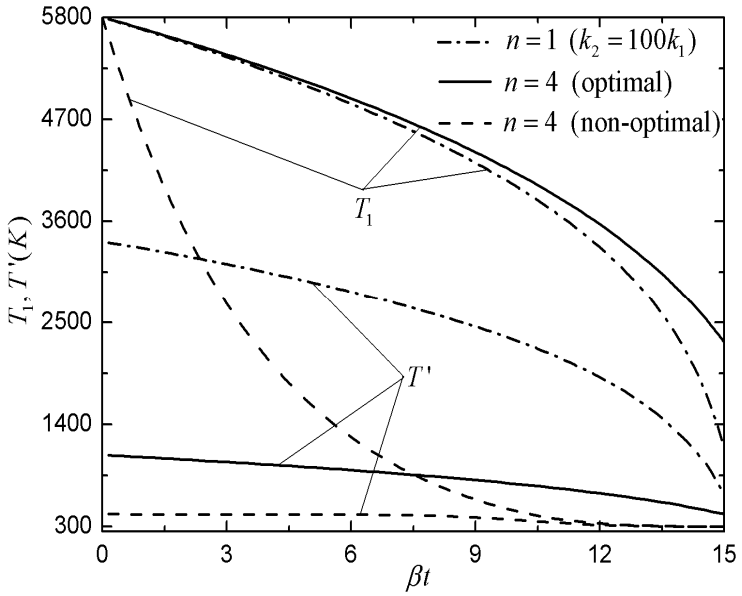

Figure 15. The optimal driving fluid temperature T_1 and optimal Carnot temperature T' versus the time βt (free T_{1f})

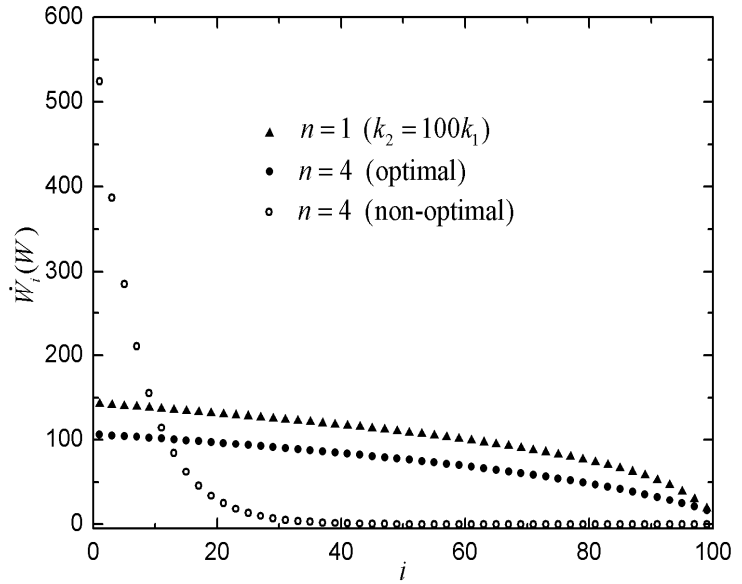

Figure 16. The optimal power output $\dot{W}_i$ of each stage heat engine versus the stage i (free T_{1f})

6. Conclusion

On the basis of Refs. [5, 7, 11, 13-22, 34-44], this paper further investigates the multistage endoreversible Carnot heat engine system operating between a finite thermal capacity high-temperature fluid reservoir and an infinite thermal capacity low-temperature environment with the heat transfer law [$q \propto \alpha(T^{4-n})(\Delta(T^n))$]. Optimal control theory is applied to derive the continuous HJB equations, which determined the optimal fluid temperature configurations for maximum power output under the conditions of fixed duration and fixed initial temperature of the driving fluid. Based on universal optimization results, the analytical solution for the pseudo-Newtonian heat transfer law [$q \propto \alpha(T^3)(\Delta T)$] is also obtained. Since there are no analytical solutions for the radiative heat transfer law [$q \propto \Delta(T^4)$], the continuous HJB equations are discretized and the dynamic programming algorithm is adopted to obtain the complete numerical solutions of the optimization problem. Numerical examples for the radiative heat transfer law and two different boundary conditions including the free and fixed final temperatures are given, and the obtained results are also compared with those for the pseudo-Newtonian heat transfer law and the results for the stage-by-stage optimization strategy. The results show that when the final fluid temperature is fixed, optimization for maximizing power output is equivalent to that for minimizing entropy generation rate, besides, if the process period tends to infinity, the maximum power output of the multistage endoreversible heat engine system tends to its reversible power performance limit; when both the process period and the final fluid temperature are fixed, there is an optimal control strategy for the power output of the multistage heat engine system to achieve its maximum value, and the maximum power output and the corresponding optimal driving fluid temperature configuration are different for different final fluid temperature; when the final fluid temperature is free, optimization for maximizing power output is not equivalent to that for minimizing entropy generation rate, however, if the process period is fixed further, there is an optimal final fluid temperature for the power output of the multistage heat engine system to achieve its maximum value, the total time constraint has effects on the optimal driving fluid temperature configuration, the maximum power output and the corresponding optimal control strategy; when the process period and the final fluid temperature tend to infinity and the environment temperature, respectively, the maximum power output of the multistage endoreversible heat engine system tends to the classical radiation thermodynamic exergy function; both the maximum power output of the multistage heat engine system and the corresponding optimal fluid temperature configuration for the radiative heat transfer law are significantly different from those for the pseudo-Newtonian heat transfer law, and the power output for the global optimization strategy with the radiative heat transfer law is 93% larger than that for the stage-by-stage optimization strategy. The obtained results can provide some theoretical guidelines for the optimal designs and operations of solar energy conversion and transfer systems.

Appendix A

The dimensionless time τ is defined as follows:

$$\tau = [(k_1 T_1^3)/(k_2 T_2^3)+1]t/(4\beta) \tag{A1}$$

Eqs. (25), (30) and (31), respectively, become

$$dT_1/d\tau = T' - T_1 \tag{A2}$$

$$\frac{\partial \dot{W}^I_{\max}}{\partial \tau} + \max_{T'(t)\in\Omega}\{[GC_h(1-\frac{T_2}{T'}) - \frac{\partial W^I_{\max}}{\partial T_1}](T_1 - T')\} = 0 \tag{A3}$$

$$\frac{\partial \dot{W}^{II}_{\max}}{\partial \tau} + \max_{T'(t)\in\Omega}\{[(GC_h - GC_V\frac{T_2}{T'}) - \frac{\partial W^{II}_{\max}}{\partial T_1}](T_1 - T')\} = 0 \tag{A4}$$

(a) $\dot{W}^I_{\max}$ is chosen to be optimization objective

Maximizing the second term of Eq. (A3) with respect to T' yields

$$T^{'}=\sqrt{T_1T_2/[1-(GC_h)^{-1}(\partial\dot{W}^I_{\max}/\partial T_1)]} \tag{A5}$$

Substituting Eq. (A5) into Eq. (A3) yields

$$\frac{\partial\dot{W}^I_{\max}}{\partial\tau}+\left\{GC_hT_1\{\sqrt{[1-(GC_h)^{-1}(\partial\dot{W}^I_{\max}/\partial T_1)]}-\sqrt{T_2/T_1}\}^2\right\}=0 \tag{A6}$$

The second term of Eq. (A6) is the extremum Hamilton function $H(T_1,\partial\dot{W}^I_{\max}/\partial T_1)$

$$H(T_1,\partial\dot{W}^I_{\max}/\partial T_1)=GC_hT_1\{\sqrt{[1-(GC_h)^{-1}(\partial\dot{W}^I_{\max}/\partial T_1)]}-\sqrt{T_2/T_1}\}^2 \tag{A7}$$

From Eq. (A7), one can see that H contains the variable τ inexplicitly, and the equation $dH/d\tau=\partial H/\partial\tau$ holds for the Hamilton function, so the Hamilton function is autonomous and $H(T_1,\partial\dot{W}^I_{\max}/\partial T_1)$ keeps constant along the optimal path. Let the constant be h, and one further obtains

$$GC_hT_1\{\sqrt{[1-(GC_h)^{-1}(\partial\dot{W}^I_{\max}/\partial T_1)]}-\sqrt{T_2/T_1}\}^2=h \tag{A8}$$

Solving Eq. (A8) for $\partial\dot{W}^I_{\max}/\partial T_1$ yields

$$\partial\dot{W}^I_{\max}/\partial T_1=GC_h\{1-\{\sqrt{h/(GC_hT_1)}+\sqrt{T_2/T_1}\}^2\} \tag{A9}$$

Substituting Eq. (A9) into Eq. (A3) yields

$$T^{'}=\frac{T_1}{\sqrt{h/(GC_hT_2)}+1} \tag{A10}$$

Substituting Eq. (A10) into Eq. (A2) yields

$$\frac{dT_1}{d\tau}=\frac{-\sqrt{h/(GC_hT_2)}}{\sqrt{h/(GC_hT_2)}+1}T_1 \tag{A11}$$

Since $T_1(\tau_i)=T_{1i}$, substituting $GC_h=64\dot{V}\sigma_BT_1^3/(3c)$ into Eq. (A11) and then integrating it yields the optimal working fluid temperature T_1 versus the time τ:

$$-\frac{16}{3}\sqrt{\frac{\dot{V}\sigma_BT_2}{3ch}}(T_1^{3/2}-T_{1i}^{3/2})-\ln(T_1/T_{1i})=\tau-\tau_i \tag{A12}$$

Substituting Eqs. (A10) and (A11) into Eq. (18) yields

$$\sigma^I_s=\frac{16}{3}\sqrt{\frac{h\dot{V}\sigma_B}{3cT_2}}(T_{1i}^{3/2}-T_{1f}^{3/2}) \tag{A13}$$

The maximum power output $\dot{W}^I_{\max}$ is given by

$$\begin{aligned}\dot{W}^I_{\max}&=\frac{16\dot{V}\sigma_B(T_{1i}^4-T_{1f}^4)}{3c}-\frac{64\dot{V}\sigma_BT_2(T_{1i}^3-T_{1f}^3)}{9c}-\frac{16T_2}{3}\sqrt{\frac{h\dot{V}\sigma_B}{3cT_2}}(T_{1i}^{3/2}-T_{1f}^{3/2})\\&=\dot{W}^I_{rev}-T_2\sigma^I_s\end{aligned} \tag{A14}$$

Eqs. (A12)-(A14) coincides with the results obtained by variational calculus in Refs. [11, 35-40].

(b) $\dot{W}_{\max}^{II}$ is chosen to be optimization objective

Maximizing the second term of Eq. (A4) with respect to T' yields

$$T' = \sqrt{GC_V T_1 T_2 / [GC_h - (\partial \dot{W}_{\max}^{II} / \partial T_1)]} \tag{A15}$$

Substituting Eq. (A15) into Eq. (A4) yields

$$\frac{\partial \dot{W}_{\max}^{II}}{\partial \tau} + \{\sqrt{[GC_h - (\partial \dot{W}_{\max}^{II} / \partial T_1)]T_1} - \sqrt{GC_V T_2}\}^2 = 0 \tag{A16}$$

The second term of Eq. (A6) is the extremum Hamilton function $H(T_1, \partial \dot{W}_{\max}^{II} / \partial T_1)$

$$H(T_1, \partial \dot{W}_{\max}^{II} / \partial T_1) = \{\sqrt{[GC_h - (\partial \dot{W}_{\max}^{II} / \partial T_1)]T_1} - \sqrt{GC_V T_2}\}^2 \tag{A17}$$

From Eq. (A17), one can see that H contains the variable τ inexplicitly, and the equation $dH / d\tau = \partial H / \partial \tau$ holds for the Hamilton function, so the Hamilton function is autonomous and $H(T_1, \partial \dot{W}_{\max}^{II} / \partial T_1)$ keeps constant along the optimal path. Let the constant be h, and one further obtains

$$\{\sqrt{[GC_h - (\partial \dot{W}_{\max}^{II} / \partial T_1)]T_1} - \sqrt{GC_V T_2}\}^2 = h \tag{A18}$$

Solving Eq. (A18) for $\partial \dot{W}_{\max}^{II} / \partial T_1$ yields

$$\partial \dot{W}_{\max}^{II} / \partial T_1 = GC_h - (\sqrt{h} + \sqrt{GC_V T_2})^2 / T_1 \tag{A19}$$

Substituting Eq. (A19) into Eq. (A15) yields

$$T' = \frac{T_1}{1 + \sqrt{h / (GC_V T_2)}} \tag{A20}$$

Substituting Eq. (A20) into Eq. (A2) yields

$$dT_1 / d\tau = -\frac{\sqrt{h / (GC_V T_2)}}{\sqrt{h / (GC_V T_2)} + 1} T_1 \tag{A21}$$

Since $T_1(\tau_i) = T_{1i}$, substituting $GC_V = 16\dot{V}\sigma_B T_1^3 / c$ into Eq. (A21) and then integrating it yields the optimal working fluid temperature T_1 versus the time τ:

$$-\frac{8}{3}\sqrt{\frac{\dot{V}\sigma_B T_2}{ch}}(T_1^{3/2} - T_{1i}^{3/2}) - \ln(T_1 / T_{1i}) = \tau - \tau_i \tag{A22}$$

Substituting Eqs. (A20) and (A21) into Eq. (20) yields

$$\sigma_s^{II} = \frac{8}{3}\sqrt{\frac{\dot{V}\sigma_B h}{cT_2}}(T_{1i}^{3/2} - T_{1f}^{3/2}) \tag{A23}$$

The maximum power output $\dot{W}_{\max}^{II}$ is given by

$$\dot{W}_{\max}^{II} = \frac{16\dot{V}\sigma_B(T_{1i}^4 - T_{1f}^4)}{3c} - \frac{16\dot{V}\sigma_B T_2(T_{1i}^3 - T_{1f}^3)}{3c} - \frac{8T_2}{3}\sqrt{\frac{\dot{V}\sigma_B h}{cT_2}}(T_{1i}^{3/2} - T_{1f}^{3/2}) \quad \text{(A24)}$$
$$= \dot{W}_{rev}^{II} - T_2\sigma_s^{II}$$

Acknowledgements

This paper is supported by the National Natural Science Foundation of P. R. China (Project No. 10905093), the Program for New Century Excellent Talents in University of P. R. China (Project No. NCET-04-1006) and the Foundation for the Author of National Excellent Doctoral Dissertation of P. R. China (Project No. 200136).

References

[1] Andresen B, Berry R S, Ondrechen M J, Salamon P. Thermodynamics for processes in finite time. Acc. Chem. Res., 1984, 17(8): 266-271.
[2] Bejan A. Entropy generation minimization: The new thermodynamics of finite-size devices and finite-time processes. J. Appl. Phys., 1996, 79(3): 1191-1218.
[3] Berry R S, Kazakov V A, Sieniutycz S, Szwast Z, Tsirlin A M. Thermodynamic Optimization of Finite Time Processes. Chichester: Wiley, 1999.
[4] Chen L, Wu C, Sun F. Finite time thermodynamic optimization or entropy generation minimization of energy systems. J. Non-Equilib. Thermodyn., 1999, 24(4): 327-359.
[5] Sieniutycz S. Hamilton-Jacobi-Bellman framework for optimal control in multistage energy systems. Phys. Rep., 2000, 326(4): 165-285.
[6] Hoffman K H, Burzler J, Fischer A, Schaller M, Schubert S. Optimal process paths for endoreversible systems. J. Non-Equilib. Thermodyn., 2003, 28(3): 233-268.
[7] Sieniutycz S. Thermodynamic limits on production or consumption of mechanical energy in practical and industry systems. Progress Energy Combus. Sci., 2003, 29(3): 193-246.
[8] Chen L, Sun F. Advances in Finite Time Thermodynamics: Analysis and Optimization. New York: Nova Science Publishers, 2004.
[9] Chen L. Finite-Time Thermodynamic Analysis of Irreversible Processes and Cycles (in Chinese). Beijing: High Education Press, 2005.
[10] Andresen B. The need for entropy in finite-time thermodynamics and elsewhere. Meeting the Entropy Challenge: An International Thermodynamics Symposium in Honor and Memory of Professor Joseph H. Keenan, AIP Conference Proceedings, Volume 1033, 2008, pp. 213-218.
[11] Sieniutycz S, Jezowski J. Energy Optimization in Process Systems. Elsevier, Oxford, UK, 2009
[12] Andresen B. Current Trends in Finite-Time Thermodynamics. Angew. Chem. Int. Ed., 2011, 50(12): 2690-2705.
[13] Sieniutycz S. Hamilton-Jacobi-Bellman theory of dissipative thermal availability. Phys. Rev. E, 1997, 56(5): 5051-5064.
[14] Sieniutycz S. Irreversible Carnot problem of maximum work in a finite time via Hamilton-Jacobi-Bellman theory. J. Non-Equib. Thermodyn., 1997, 22(3): 260-284.
[15] Sieniutycz S. Nonlinear thermokinetics of maximum work in finte time. Int. J. Engng Sci., 1998, 36(5-6): 577-597.
[16] Sieniutycz S. Endoreversible modeling and optimization of multi-stage thermal machines by dynamic programming. In Recent Advances in Finite Time Thermodynamics, Eds. Wu C, Chen L, Chen J. Nova Science Publishers, New York, 1999, 189-219.
[17] Sieniutycz S, von Spakovsky M R. Finite time generalization of thermal exergy. Energy Convers. Mgmt., 1998, 39(14):1423-1447.
[18] Szwast Z, Sieniutycz S. Optimization of multi-stage thermal machines by Pontryagin's like discrete maximum principle. In Recent Advances in Finite Time Thermodynamics, Eds. Wu C, Chen L, Chen J. Nova Science Publishers, New York, 1999, 221-237.
[19] Sieniutycz S, Szwast Z. Work limits in imperfect sequential systems with heat and fluid flow. J. Non-Equilib. Thermodyn., 2003, 28(2): 85-114.
[20] Sieniutycz S. Development of generalized (rate dependent) availability. Int. J. Heat Mass Transfer, 2006, 49(3-4): 789-795.
[21] Li J, Chen L, Sun F. Extremal work of an endoreversible system with two finite thermal capacity reservoirs. J. Energy Ins., 2009, 82(1): 53-56.

[22] Li J, Chen L, Sun F. Optimum work in real systems with a class of finite thermal capacity reservoirs. Math. Comp. Model., 2009, 49(3/4): 542-547.
[23] Gutowicz-Krusin D, Procaccia J, Ross J. On the efficiency of rate processes: Power and efficiency of heat engines. J. Chem. Phys., 1978, 69(9): 3898-3906.
[24] de Vos A. Efficiency of some heat engines at maximum power conditions. Am. J. Phys., 1985, 53(6): 570-573.
[25] Angulo-Brown F, Paez-Hernandez R. Endoreversible thermal cycle with a nonlinear heat transfer law. J. Appl. Phys., 1993, 74(4): 2216-2219.
[26] Zhou S, Chen L, Sun F. Optimal performance of a generalized irreversible Carnot engine. Appl. Energy, 2005, 81(4): 376-387.
[27] Huleihil M, Andresen B. Convective heat transfer law for an endoreversible engine. J. Appl. Phys., 2006, 100(1): 014911.
[28] Chen L, Xia S, Sun F. Optimal paths for minimizing entropy generation during heat transfer processes with a generalized heat transfer law. J. Appl. Phys., 2009, 105(4): 044907.
[29] Xia S, Chen L, Sun F. Optimal paths for minimizing entransy dissipation during heat transfer processes with generalized radiative heat transfer law. Appl. Math. Model., 2010, 34(8): 2242-2255.
[30] Song H, Chen L, Sun F. Optimal configuration of a class of endoreversible heat engines for maximum efficiency with radiative heat transfer law. Sci China Ser G: Phys, Mech & Astron, 2008, 51(9): 1272-1286.
[31] Chen L, Zhu X, Sun F, Wu C. Optimal configurations and performance for a generalized Carnot cycle assuming the heat transfer law $Q \propto (\Delta T)^m$. Appl. Energy, 2004, 78(3): 305-313.
[32] Xia S, Chen L, Sun F. The optimal path of piston motion for Otto cycle with linear phenomenological heat transfer law. Sci. China Ser. G: Phys, Mech & Astron, 2009, 52(4): 708-719.
[33] Xia S, Chen L, Sun F. Maximum power output of a class of irreversible non- regeneration heat engines with a non-uniform working fluid and linear phenomenological heat transfer law. Sci. China Ser. G: Phys, Mech & Astron, 2009, 52(5): 1961-1970.
[34] Sieniutycz S, Kuran P. Nonlinear models for mechanical energy production in imperfect generators driven by thermal or solar energy. Int. J. Heat Mass Transfer, 2005, 48(3-4): 719-730.
[35] Sieniutycz S, Kuran P. Modeling thermal behavior and work flux in finite-rate systems with radiation. Int. J. Heat Mass Transfer, 2006, 49(17-18): 3264-3283.
[36] Kuran P. Nonlinear Models of Production of Mechanical Energy in Non-ideal Generators Driven by Thermal or Solar Energy. Ph. D. Thesis, Warsaw University of Technology, Poland, 2006.
[37] Sieniutycz S. Hamilton–Jacobi–Bellman equations and dynamic programming for power-maximizing relaxation of radiation. Int. J. Heat Mass Transfer, 2007, 50(13-14): 2714-2732.
[38] Sieniutycz S. Dynamical converters with power-producing relaxation of solar radiation. Int. J. Thermal Sci, 2008, 47(4): 495-505.
[39] Sieniutycz S. Dynamic programming and Lagrange multipliers for active relaxation of resources in nonlinear non-equilibrium systems. Appl. Math. Model., 2009, 33(3): 1457-1478.
[40] Sieniutycz S. Finite-rate thermodynamics of power production in thermal, chemical and electrochemical systems. Int. J. Heat Mass Transfer, 2010, 53(13-14): 2864-2876.
[41] Sieniutycz S. Dynamic bounds for power and efficiency of non-ideal energy converters under nonlinear transfer laws. Energy, 2009, 34(3): 334-340.
[42] Li J, Chen L, Sun F. Maximum work output of multistage continuous Carnot heat engine system with finite reservoirs of thermal capacity and radiation between heat source and working fluid. Thermal Sci., 2011, 14(1): 1-9.
[43] Xia S, Chen L, Sun F. Hamilton–Jacobi–Bellman equations and dynamic programming for power-optimization of multistage heat engine system with generalized convective heat transfer law. Chin. Sci Bull, 2011, 56(11): 1147-1157.
[44] Xia S, Chen L, Sun F. Power-optimization of non-ideal energy converters under generalized convective heat transfer law via Hamilton-Jacobi-Bellman theory. Energy, 2011, 36(1): 633-646.
[45] Vollmer M. Newton's law of cooling revisited. Eur. J. Phys., 2009, 30(5): 1063-1084.
[46] Sieniutycz S. Carnot controls to unify traditional and work-assisted operation with heat and mass transfer. Int. J. Thermodyn., 2003, 6(2):1-9.

[47] Bejan A. Unification of three different theories concerning the ideal conversion of enclosed radiation, J. Solar Energy Engng., 1987, 109(1): 46-51.
[48] Petela R, Exergy of undiluted thermal radiation, Solar Energy, 2003, 74(6): 469-488.
[49] Chen Z, Mo S, Hu P. Radiation thermodynamics—Availability of radiation, Equivalent temperature and entropy constant of photon. Sci. China ser-E: Tech. Sci., 2009, 39(4): 609-617.
[50] de Vos A. Thermodynamics of Solar Energy Conversion. Wiley--VCH Verlag, 2008.
[51] V. Badescu. Letter to the Editor, Solar Energy, 2004, 20: 149-160.
[52] Bellman R E. Adaptive Control Processes: a Guided Tour. Princeton: Princeton University Press, 1961.
[53] Hu S, Wang Z, Hu W. Optimal control theory and system (in Chinese). Beijing: Science Press, 2005.

Shaojun Xia received his BS degree from the Naval University of Engineering, P R China in 2007. He is pursuing for his PhD in power engineering and engineering thermophysics from Naval University of Engineering, P R China. His work covers topics in finite time thermodynamics and technology support for propulsion plants. He is the author or coauthor of over 25 peer-refereed papers (over 23 in English).

Lingen Chen received all his degrees (BS, 1983; MS, 1986, PhD, 1998) in power engineering and engineering thermophysics from the Naval University of Engineering, P R China. His work covers a diversity of topics in engineering thermodynamics, constructal theory, turbomachinery, reliability engineering, and technology support for propulsion plants. He had been the Director of the Department of Nuclear Energy Science and Engineering, the Director of the Department of Power Engineering and the Superintendent of the Postgraduate School. Now, he is the Dean of the College of Naval Architecture and Power, Naval University of Engineering, P R China. Professor Chen is the author or coauthor of over 1200 peer-refereed articles (over 510 in English journals) and nine books (two in English).
E-mail address: lgchenna@yahoo.com; lingenchen@hotmail.com, Fax: 0086-27-83638709 Tel: 0086-27-83615046

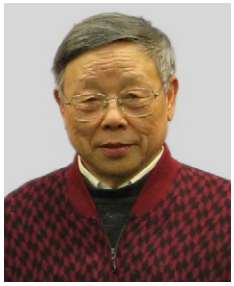

Fengrui Sun received his BS Degrees in 1958 in Power Engineering from the Harbing University of Technology, PR China. His work covers a diversity of topics in engineering thermodynamics, constructal theory, reliability engineering, and marine nuclear reactor engineering. He is a Professor in the Department of Power Engineering, Naval University of Engineering, PR China. He is the author or co-author of over 950 peer-refereed papers (over 440 in English) and two books (one in English).

